The effect of scattering calculations on non-LTE modelling of the C 3 O and C 5 O abundances in TMC-1

C Bop, F Khadri, K Hammami

The effect of scattering calculations on non-LTE modelling of the C_3O and C_5O abundances in TMC-1

C. T. Bop,[1]★ F. Khadri,[2]† K. Hammami[2]
[1] Univ Rennes, CNRS, IPR (Institut de Physique de Rennes) - UMR 6251, F-35000 Rennes, France
[2] LSAMA, Departement of Physics, Faculty of Sciences, Université Tunis El-Manar, 1060 Tunis, Tunisia

Accepted XXX. Received YYY; in original form ZZZ

ABSTRACT

Tricarbon and pentacarbon monoxides have been detected towards TMC-1 with relatively important abundances. Understanding their chemical formation of these molecules requires interpreting their observational spectra by mean of non-local thermodynamical equilibrium modelling. For this purpose, we report rate coefficients of C_3O and C_5O induced by collision with He for temperatures up to 100 K. These data are obtained by calculating inelastic cross sections for the 31 low-lying rotational levels of C_3O and C_5O using the close-coupling approach. The comparison of the new rate coefficients with those of HC_3N and HC_5N, previously used to interpret the observational spectra of C_3O and C_5O, reveals differences of up to an order of magnitude. The effect of the new collisional rate coefficients in radiative transfer calculations is checked by computing the excitation temperatures for some transitions and simulating the C_3O and C_5O column densities observed towards TMC-1. Our findings suggest that the use of HC_nN as template for C_nO may lead to local thermodynamic equilibrium conditions for gas densities as low as $\sim 10^3$ cm^{-3}. Regarding the interpretation of the observational spectra, using radiative transfer modelling based on the actual C_nO collisional rate coefficients instead of rotational diagram analysis leads to underestimate the column densities reported in the literature by up to 25% and accordingly the C_3O/C_5O abundance ratio by up to 50%. We expect that the new rate coefficients and the radiative transfer calculations presented in this work will encourage further modellings of the C_nO abundance and accordingly constrain the chemistry.

Key words: ISM: molecules – molecular data – scattering

1 INTRODUCTION

During the last decades, important theoretical and experimental progresses were made to determine high accurate molecular spectroscopic data such as electric dipole moment and rotational constant. These pieces of information are crucial to identify interstellar molecules through their observational spectra. For instance, the detection of l-HC_3^+ towards the Horsehead nebula (Pety et al. 2012) was questioned by *ab initio* calculations (Huang et al. 2013) then confirmed by laboratory measurements (Brünken et al. 2014).

Thanks to these efforts, TMC-1 is now known as an astronomical source particularly rich of carbon chain molecules such as C_nN (Friberg et al. 1980; Guélin et al. 1998), C_nS (Cernicharo et al. 2021a) and especially C_nO ($n \geq 3$) whose chemical growth remains to be understood. C_3O was first detected by Matthews et al. (1984) through its $2 \rightarrow 1$ rotational emission line towards TMC-1, then Brown et al. (1985) detected the $5 \rightarrow 4$, $8 \rightarrow 7$ and $9 \rightarrow 8$ lines in the same region. Furthermore, this molecule was identified towards different astronomical sources, namely the carbon rich circumstellar envelope IRC +10216 (Tenenbaum et al. 2006), the low-mass protostar ELIAS 18 (Palumbo et al. 2008) and the prestellar core L1544 (Vastel et al. 2014). Recently, Cernicharo et al. (2021b) reported the discovery of C_5O in TMC-1. These authors detected 6 emission lines involving only high-lying rotational energy levels, i.e. $j = 12 - 17 \rightarrow 11 - 16$. Therefore, highly accurate determination of C_3O and C_5O abundances can lead to a better understanding of the C_nO chemistry in TMC-1.

The column densities of C_3O and C_5O observed towards TMC-1 were determined by mean of rotational diagram analysis of the observational spectra (Cernicharo et al. 2021b), i.e. by assuming that local thermodynamic equilibrium (LTE) conditions are reached. The use of such an approximation is motivated by the lack of collisonal data for C_3O and C_5O even though LTE conditions are rarely verified in the ISM. To check the validity of their assumption, Cernicharo et al. (2021b) calculated excitation temperatures for the observed lines under the large velocity gradient (LVG) approach adopting collisional rate coefficients of HC_3N and HC_5N as template for C_3O and C_5O, respectively. Despite the similarity of the C_nO and HC_nN electronic structures, the impact of the actual C_nO collisional rate coefficients in the abundance determination deserves to be assessed.

Collisional excitation of CO, the simplest member of the C_nO family, by He has been extensively investigated both theoretically and experimentally. For example, using a potential energy surface (PES) based on the electron-gas model, Green & Thaddeus (1976) calculated collisional rate coefficients up to 100 K for the low-lying

★ E-mail:cheikhtidiane.bop@ucad.edu.sn
† E-mail: fehmi.khadri@fst.utm.tn

rotational energy levels of CO–He and CO–H_2. Subsequently, using a high accurate *ab initio* potential computed by Heijmen et al. (1997), Cecchi-Pestellini et al. (2002) reported CO rate coefficients due to collision with He for temperatures up to 500 K. Nevertheless, C_3O received less attention despite its early discovery towards TMC-1 (Matthews et al. 1984).

Collisional excitation of C_3O (Khadri & Hammami 2019) and C_5O (Khadri et al. 2022) by He was studied recently by mean of state-of-the-art methods. New 2D-PESs were calculated using high accurate *ab initio* level of theories. Based on the latter data, collisional rate coefficients for the 12 (20) low-lying rotational levels of C_3O–He (C_5O–He) were derived for temperatures up to 25 K (100 K). Since C_3O and especially C_5O were detected through rotational emission lines involving high-lying energy levels (up to $11 \rightarrow 10$ for C_3O and $17 \rightarrow 16$ for C_5O) we revisit the excitation of these molecules induced by collision with He to provide a complete set of data. In fact, modelling the $11 \rightarrow 10$ (for C_3O) and $17 \rightarrow 16$ (for C_5O) requires accounting for contributions from populations of rotational levels as high as 20 and 30, respectively.

The use of He as collision partner is usual in the literature since it provides rough estimates for *para*-$H_2(j_2{}^1 = 0)$, i.e. the most abundant species in the ISM and especially in TMC-1 where C_3O and C_5O were observed. Both projectiles are closed-shell, spherical and two-valence-electron species. Therefore, rate coefficients induced by collision with He can be multiplied by the mass scaling factor to roughly estimate those due to *para*-$H_2(j_2 = 0)$ impact. Indeed, Wernli et al. (2007) showed an average ratio of ~ 1.4 between the HC_3N–*para*-$H_2(j_2 = 0)$ and HC_3N–He collisional rate coefficients. This finding for an HC_nN-type molecule, let us expect a reasonably good agreement in the case of C_nO, .i.e the isoelectronic compounds. However, we anticipate by warning that this approximation is limited especially for charged species and hydrides.

This paper is structured as follows: Section 2 presents the computational details, in Section 3 we discus the results and Section 4 gives the concluding remarks

2 METHODS

2.1 Analytical fit

The data reported in this work are calculated using the potential energy surfaces (PESs) of the C_3O–He and C_5O–He complexes (Khadri & Hammami 2019; Khadri et al. 2022). Briefly, the PESs are calculated at the CCSD(T)-F12[2]/aug-cc-pVTZ[3] level of theory using the rigid-rotor approximation. Since the electronic calculations are out of the scope of this work, we refer the readers to the papers mentioned above.

To obtain collisional rate coefficients for higher rotational levels of C_3O and C_5O, we determine new analytical fits of the *ab initio* potentials including few radial terms (V_λ) to keep the computational time reasonably low. In fact, due to the rod-like shape of the C_nO molecules, Khadri & Hammami (2019) and Khadri et al. (2022) used 77 and 72 terms to reproduce reasonably well the *ab initio* PESs of C_3O and C_5O, respectively. To reduce the number of radial terms without losing precision on the analytical potentials, we used

[1] rotational quantum number of H_2

[2] explicitly correlated coupled cluster approach with single, double and perturbative triple excitation

[3] augmented-correlation consistent-polarised valence triple zeta Gaussian basis set

Table 1. State-to-state inelastic cross sections (in unit of $\AA^2$) of C_3O and C_5O computed at 100 cm^{-1} using the old $^{(a,b)}$ and new analytical PESs.

line	C_3O		C_5O	
$1 \rightarrow 0$	6.78^a	6.78	10.72^b	10.75
$5 \rightarrow 3$	4.14^a	4.14	7.99^b	8.00
$10 \rightarrow 7$	2.23^a	2.23	2.10^b	2.14

$^{(a)}$ stands for Khadri & Hammami (2019).
$^{(b)}$ stands for Khadri et al. (2022).

the weighted least square multiple regression method (Filliben & Heckert 2002) in the expansion of the *ab initio* PESs over Legendre polynomials:

$$V(R,\theta) = \sum_{\lambda=0}^{\lambda_{\max}} V_\lambda(R) P_\lambda(cos\theta), \quad (1)$$

where R is the distance between the centers of mass of the monomers (i.e. C_nO and He) and θ stands for the scattering angle. This approach yields 35 and 27 radial coefficients for the PESs of C_3O-He and C_5O-He, respectively. The so-obtained analytical potentials are shown in Fig. 1, they are identical to the interpolated *ab initio* PESs represented in the works of Khadri & Hammami (2019) and Khadri et al. (2022). It is worth noting that in this representation the linear configurations $He\cdots C_nO$ and $C_nO\cdots He$ correspond to $\theta = 0°$ and $\theta = 180°$, respectively. Both potentials (especially in the case of C_5O–He) are very anisotropic and manifest a stronger repulsion towards the carbon-end (i.e. $\theta = 0°$) and present shallow minima. Indeed, the C_5O–He PES exhibits two minima of 59.3 cm^{-1} and 53.06 cm^{-1} which are similar in magnitude to the unique global minimum of 53.4 cm^{-1} obtained for C_3O–He. Moreover, in C_nO-He ($n = 3, 5$) systems and unlike their C_nS–He valence isoelectronic counterparts (Sahnoun et al. 2020; Khadri et al. 2020), the charge distribution on the oxygen atom is negative and the Pauli exchange repulsion does not allow quasi-bonding between the O and He atoms. To check the validity of our new fit, we compare in Table 1 state-to-state inelastic cross-sections of C_3O and C_5O computed using the old (Khadri & Hammami 2019; Khadri et al. 2022) and new (this work) analytical PESs. For all transitions, slight deviations (less than 2%) are orbserved.

2.2 Cross sections and rate coefficients

The collisional processes we are studying can be sketched as follows:

$$C_nO(j) + He \quad \rightarrow \quad C_nO(j') + He \quad (2)$$

where $n = \{3, 5\}$ and j being the total angular momentum of C_nO. We report state-to-state inelastic cross sections (σ) for the 31 low-lying rotational levels of C_nO ($j = 0 - 30$). Calculations are performed for total energies ranging up to 750 cm^{-1} and 650 cm^{-1} for C_3O and C_5O, respectively. To correctly describe the resonances, we span the energy range using a fine step size of 0.1 cm^{-1} up to 200 cm^{-1} (100 cm^{-1}) for C_3O (C_5O). The calculations are performed by mean of the quantum mechanical close-coupling approach as implemented in the `MOLSCAT` computer code (Alexander 1977; Hutson & Green code).

Convergence tests are performed at the first stage to determine the integration parameters (see Table 2) which are j_{max} (the size of the rotational basis), STEPS (a parameter inversely proportional to the integration step) and R_{mid} (the switching point between the short and the long-range of the integration length).

Using a thermal average over the Maxwell-Boltzmann kinetic energy (E_k) distribution of the so-calculated cross sections, we retrieve

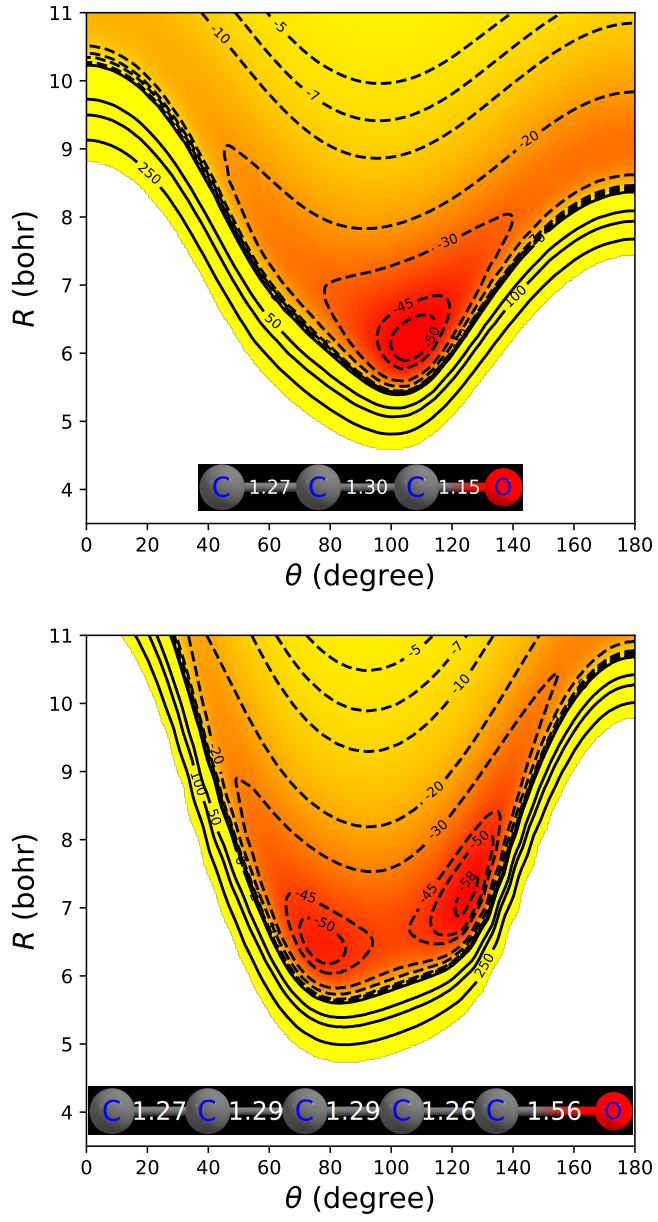

Figure 1. Contour plots of the C_3O–He (upper panel) and C_5O–He (lower panel) 2D interaction potentials (in cm^{-1}). The C_nO molecules are shown to scale and the bond distances are in *Å*.

collisional rate coefficients (k) of C_3O and C_5O for temperatures up to 100 K,

$$k_{j\rightarrow j'}(T) = (\frac{8}{\pi\mu\beta})^{1/2}\beta^2 \int_0^\infty E_k \sigma_{j\rightarrow j'}(E_k) e^{-\beta E_k}\, dE_k \qquad (3)$$

where μ is the reduced mass of C_nO–He and $\beta = (k_B T)^{-1}$ is inversely proportional to the Boltzmann constant and the temperature.

2.3 Radiative transfer study

Radiative transfer calculations are performed under the escape probability formalism, as implemented in the `RADEX` computer code (Van der Tak et al. 2007), assuming an expanding spherical shell. The basic input consists of collision rate coefficients, line frequencies, energy levels and Einstein coefficients for both C_3O and C_5O. The spectroscopic data are downloaded from the Cologne Database for Molecular Spectroscopy (CDMS) portal (Endres et al. 2016).

In this section, we calculate excitation temperature (T_{ex}), brightness temperature (T_B), integrated intensity (W) and optical depth (τ) for the detected emission lines of C_3O and C_5O and towards TMC-1 (Matthews et al. 1984; Brown et al. 1985; Cernicharo et al. 2021b). The cosmic microwave background temperature (T_{CMB} = 2.73 K) is used as background radiation field. For the full width at the half-maximum (FWHM), we use the values reported in the literature. We report in Table 3 a brief summary of the parameters of the observed emission lines including the antenna temperature (T_A^*) and the integrated intensity. Concerning physical conditions of the source of interest, i.e. TMC-1, the H_2 volume density (n) is smoothly increased from 10^2 cm^{-3} to 10^8 cm^{-3} and the gas kinetic temperature (T) is set to 10 ± 2 K as usually done in the literature (Ndaw et al. 2021; Bop et al. 2021). The column densities (N) of C_3O and C_5O are smoothly increased from 10^{10} cm^{-2} to 10^{13} cm^{-2} and 10^9 cm^{-2} to 10^{12} cm^{-2}, respectively.

Table 2. Integration parameters used in the dynamic calculations

	j_{max}	STEPS	R_{mid}
C_3O	14 – 37	10 – 80	15 a_0
C_5O	22 – 49	10 – 80	14 a_0

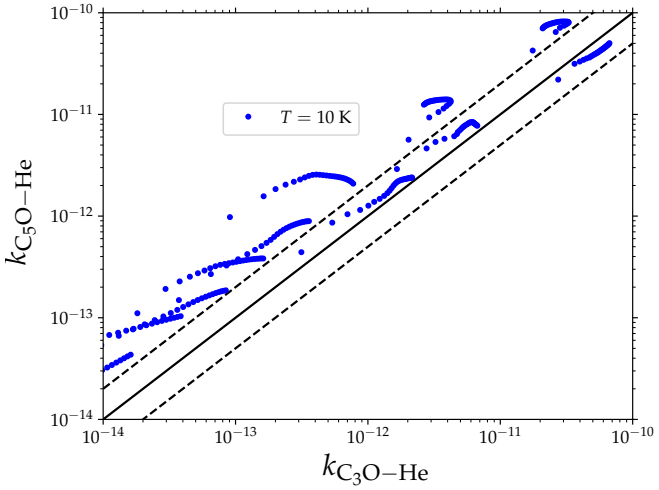

Figure 2. Comparison between collisional rate coefficients (cm^3 s^{-1}) of C_3O–He and those of C_5O–He for a temperature of 10 K. The solid diagonal line stands for $y = x$ and the dashed lines delimit an agreement of a factor of 2.

3 RESULTS

3.1 Collisional excitation of C_3O and C_5O

Fig. 2 compares rate coefficients of C_3O induced by collision with He to those of C_5O for a temperature of 10 K which corresponds to the gas kinetic temperature of TMC-1. Apart from the most dominant transitions (i.e. $\Delta j = 1$ and $k \sim 10^{-10}$ cm^3 s^{-1}), the scattering of C_5O outweighs that of C_3O. The disagreement increases up to an order of magnitude with the increase of Δj (see appendix A fore the

Table 3. Emission line parameters of the C_3O and C_5O observed towards TMC-1.

C_3O						C_5O^b			
Line	Frequency (MHz)	FWHM (km s^{-1})		T_A^* (mK)	$\int T_A^* dv$ (mK km s^{-1})	Line	Frequency (MHz)	FWHM (km s^{-1})	$\int T_A^* dv$ (mK km s^{-1})
$2 \rightarrow 1$	19243.523	0.31^a	–	36 ± 5^a	–	$12 \rightarrow 11$	32804.100	0.57	0.69 ± 0.21
$4 \rightarrow 3$	38486.891	–	0.59^b	–	38.76 ± 0.34^b	$13 \rightarrow 12$	35527.730	0.51	0.53 ± 0.15
$5 \rightarrow 4$	48108.479	0.34^a	0.65^b	162 ± 23^a	40.83 ± 0.15^b	$14 \rightarrow 13$	38271.346	0.67	0.55 ± 0.13
$8 \rightarrow 7$	76972.590	0.46^a	0.55^b	68 ± 21^a	30.31 ± 0.53^b	$15 \rightarrow 14$	41004.959	0.69	0.79 ± 0.14
$9 \rightarrow 8$	86593.685	0.43^a	0.41^b	39 ± 15^a	17.30 ± 1.40^b	$16 \rightarrow 15$	43738.562	0.95	0.57 ± 0.19
$10 \rightarrow 9$	96214.614	–	0.50^b	–	8.470 ± 0.22^b	$17 \rightarrow 16$	46472.169	0.56	0.42 ± 0.12
$11 \rightarrow 10$	105835.358	–	0.38^b	–	4.850 ± 0.71^b				

$^{(a)}$ Brown et al. (1985) and $^{(b)}$ Cernicharo et al. (2021b)

behaviour of the state-to-state rate coefficients). Similar behaviour is expected between HC_3N and HC_5N since their collisional data were used to interpret the emission lines of C_3O (Brown et al. 1985) and C_5O (Cernicharo et al. 2021b) detected towards TMC-1, respectively. Let us notice that the rate coefficients of HC_3N were reported by Green & Chapman (1978); Wernli et al. (2007) and those of HC_5N were determined using the extrapolation method suggested by Snell et al. (1981).

$$k_{HC_5N-H_2}(T) = k_{HC_3N-H_2}(T) \times \left(\frac{1}{2} + \frac{1}{2}\frac{k_{HC_3N-H_2}(T)}{k_{HCN-H_2}(T)}\right) \quad (4)$$

For both HCN (Hernández Vera et al. 2017) and HC_3N (Wernli et al. 2007) we use the rate coefficients induced by collision with *para*-H_2(j_2[4]=0).

We display in Fig. 3 the dependence on j' of rate coefficients of C_3O, HC_3N, C_5O and HC_5N induced by collision with He/H_2. As one can see, the excitation of HC_nN is much stronger than that of C_nO. Typically, the disagreement increases with the increment of Δj. For example, the data of Wernli et al. (2007) [Green & Chapman (1978)] for HC_3N–He differ to those of C_3O–He computed in this work by up to two [one] orders of magnitude. The same behaviour is observed between the rate coefficients of C_5O–He (calculated in this work and multiplied by a mass scaling factor of $\sim$ 1.38) and those of HC_5N–H_2 (obtained using equation 4). However, the use of HC_5N as substitute for C_5O leads to a larger overestimation than the use of HC_3N as template for C_3O. For example, the collisional rate coefficients of C_3O and those of HC_3N (Green & Chapman 1978) satisfy the same propensity rule, i.e. in favor of odd Δj transitions. On the other hand, the data of HC_3N (Wernli et al. 2007) [HC_5N (equation 4)] display a propensity rule in favor of even [odd] Δj transitions whereas C_3O (C_5O) favorites odd [even] Δj transitions which leads to much larger differences. In summary, the use of HC_3N (HC_5N) as template for C_3O (C_5O) is expected to alter the analysis of the observational spectra and accordingly the abundance ratio between C_3O and C_5O.

3.2 The impact of collisional rate coefficients in non-LTE modelling

To assess the effect of the new collisional rate coefficients in non-LTE radiative transfer modelling, we use the spectroscopic data of C_3O (C_5O) along with the rate coefficients of HC_3N (HC_5N) on one hand and we couple the spectroscopic data mentioned above with the actual C_3O (C_5O) rate coefficients on the other hand. These two approaches are denoted thereafter as Model (1G/W/E) and Model (2), respectively. The letter "G" ["W"] refers to collisional rate coefficients computed by Green & Chapman (1978) [Wernli et al. (2007)] and "E" stands for equation 4, respectively.

C_3O: We compare in Fig. 4 excitation temperature of C_3O computed using Model (1G/W) and Model (2). For all emission lines, Model (1G/W) leads to greater T_{ex} values than Model (2) except at low and high H_2 volume densities where we observe excellent agreements. For the $2 \rightarrow 1$ line, Model (1G) produces a suprathermal excitation at $[2 \times 10^3 - 4 \times 10^4]$ cm^{-3}, i.e. typical gas density of molecular clouds such as TMC-1, leading to an overestimation of a factor of ~ 2 with respect to Model (2).

On the other hand, the agreement obtained between the two models at low and high densities can be explained calling back the fact that the radiation field and Einstein coefficients are the same in both models. In fact, at low (high) density the molecular cloud is diffuse (dense) and the C_3O excitation is dominated by the background radiation field (Einstein coefficients).

In the intermediary region, i.e. $10^3 \leq n$ (cm^{-3}) $\leq 10^6$, the dominance of Model (1W) over Model (1G) and Model (2) can be directly related to the preponderance of k_{HC_3N} (Wernli et al. 2007) over k_{HC_3N} (Green & Chapman 1978) and k_{C_3O} (see Fig. 3).

Concerning the thermalisation of the emission lines, Model (1G/W) suggests that LTE is reached at densities lower than predicted by Model (2). This behaviour is a further evidence of the overestimation of the C_3O collisional rate coefficients due to the use of HC_3N as template in Model (1G/W). Apart from the $2 \rightarrow 1$ emission line, which is much higher due to the suprathermal effect, Model (1W) (Model (1G)) [Model (2)] predicts excitation temperatures of 5 – 10 K (5 – 9 K) [3 – 7 K] for volume densities of [1 – 4]$\times 10^4$ cm^{-2}, i.e. typical conditions for TMC-1. Indeed, considering a density of 4×10^4 cm^{-2}, Cernicharo et al. (2021b) obtained excitation temperatures of $\sim$ 10 K for the C_3O transitions involving low-lying energy levels ($j \leq 5$). These authors used Large Velocity Gradient (LVG) model adopting the HC_3N–H_2 collisional rate coefficients as template for C_3O–H_2 to check the assumption (the C_3O rotational temperature is uniform for all rotational levels) made in the analysis of the observational spectra. Let us notice that when LTE is reached, T_{ex} approaches asymptotically the gas kinetic temperature which is in these calculations 10 K. Therefore, assuming LTE conditions to interpret the emission lines of C_3O detected towards TMC-1 would lead to overestimate the excitation temperature by up to a factor of 3.

We plot also in Fig. 4 the opacity of the lines as a function of the gas volume density. As one can see, the optical depth is less than 0.1 for all emission lines which corroborates the validity of the optically thin regime. Seen that the opacity is proportional to the column density, the lines remain thin even for $N = 10^{13}$ cm^{-2}.

[4] j_2 stands for the rotational energy level of H_2.

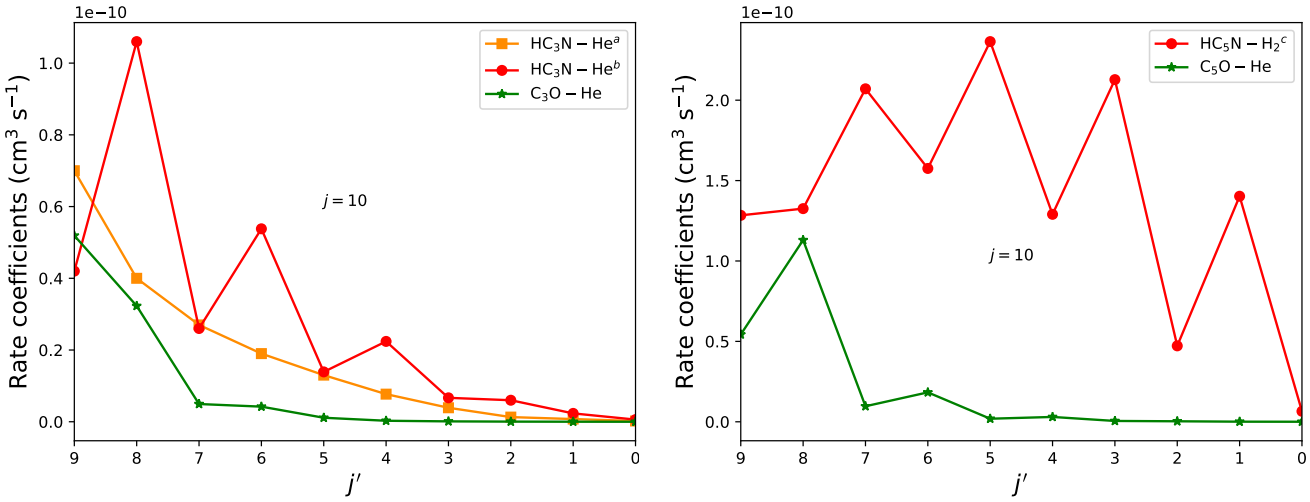

Figure 3. Comparison of collisional rate coefficients computed for temperature of 10 K: k_{C_3O--He} and $1.38 \times k_{C_5O--He}$ versus HC_3N–He and HC_5N–H_2, respectively. Superscripts $^{(a)}$ and $^{(b)}$ refer to Green & Chapman (1978) and Wernli et al. (2007), respectively whereas $^{(c)}$ stands for extrapolation obtained using equation 4

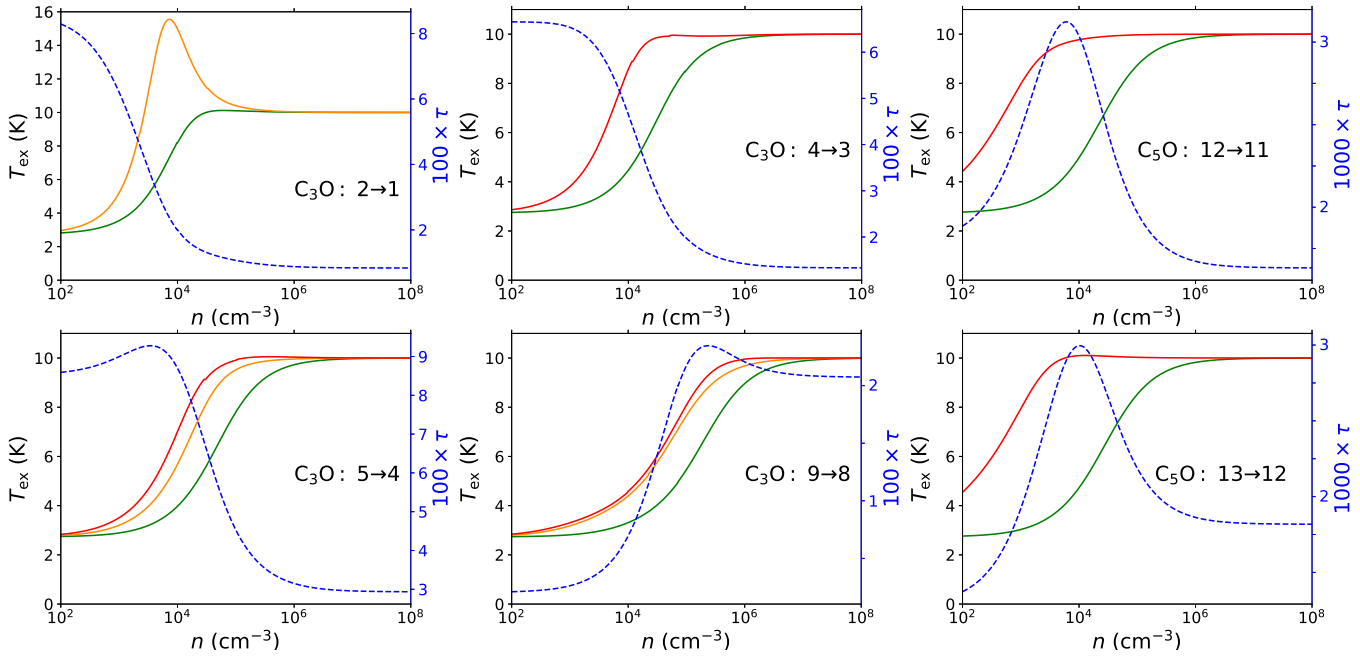

Figure 4. Dependence on volume density of C_3O and C_5O excitation temperatures. The data are computed using Model (1W) (red solid lines), Model (1G) (orange solid lines), Model (1E) (red solid line) and Model (2) (green solid line). The blue dashed lines represent the opacity calculated using Model (2) but scaled up by factors of 100 (C_3O) and 1000 (C_5O) for clarity reasons. The emission lines are shown in the panels. For C_3O (C_5O), T and N are set to 10 K and 10^{12} cm^{-2} (10 K and 10^{11} cm^{-2}), respectively.

C_5O: In this section, we briefly discuss the use of Model (1E) instead of Model (2) to interpret the C_5O emission lines. The comparison between the models does not change much depending on the molecule.

Only the 12 → 11 and 13 → 12 lines are shown in Fig. 4 since the behaviour is the same for transitions involving upper energy levels (j = 14 – 17). The HC_5N–H_2 rate coefficients are so large that T_{ex} computed with Model (1E) is much greater than T_{CMB} at $n = 10^2$ cm^{-3}. In addition, this model predicts thermalization for $n \leq 10^4$ cm^{-3} for all lines whereas Model (2), which uses the actual rate coefficients of C_5O, indicates that LTE is reached only for $n \geq 10^6$ cm^{-3}. For example, for a density of $[1-4] \times 10^4$ cm^{-3}, Model (1E) and Model (2) lead to excitation temperatures of ∼ 10 K and [5 – 7] K, respectively. Indeed, to check the validity of the rotational diagram analysis, Cernicharo et al. (2021b) obtained T_{ex} of [9.5 – 10.0] K. The latter authors used LVG calculations along with the HC_5N rate coefficients (i.e. a model which is similar to Model (1E)) adopting a density of 4×10^4 cm^{-3} and a kinetic temperature of 10 K. Therefore, the use Model (1E) validates the rotational diagram analysis whereas Model (2) strongly suggests non-LTE modelling.

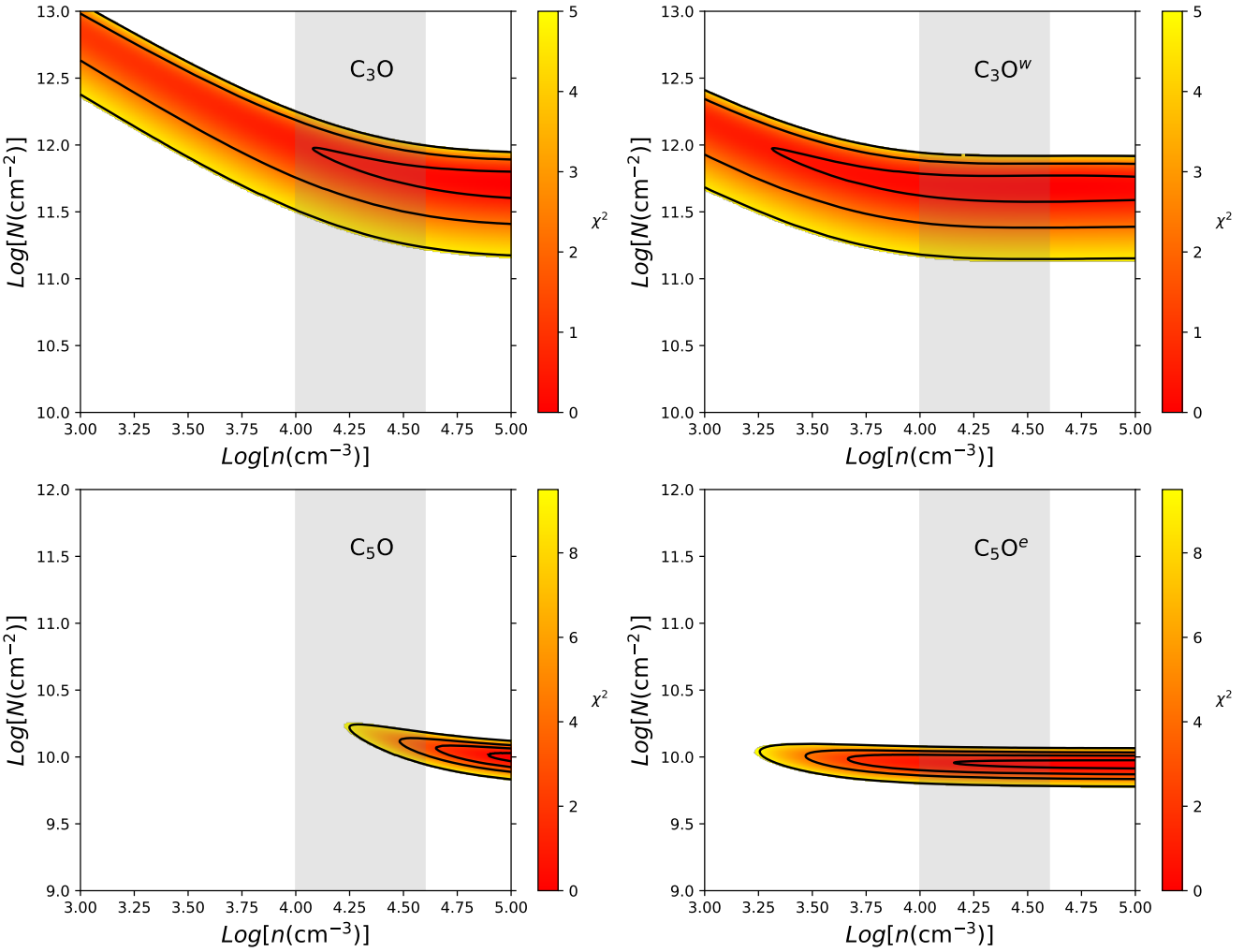

Figure 5. Dependence on H_2 volume density and C_3O (C_5O) column density of the χ^2-parameter for a kinetic temperature of 10 ± 2 K. The contour plots, from the inner to the outer, represent confidence levels of 20%, 68%, 90% and 99%. The shaded area show the typical gas density of TMC-1. The letters "w" and "e" stand for Model (1W) and Model (1E) respectively.

3.3 Interpretation of the C_3O and C_5O observational spectra

We do not claim to interpret the observational spectra of C_3O and C_5O using the most rigorous model but to assess the impact of the new rate coefficients in the $N(C_3O)/N(C_5O)$ abundance ratio. Therefore, we assume for all emission lines that the source fills the beam. We consider the main beam brightness temperature as being the antenna temperature. Ignoring the filling factor and the telescope beam and forward efficiencies does not affect our analysis since we proceed the same way for both models [Model (1E/W) and Model (2)].

We use the parameters described in Sec. 2.3 to reproduce the integrated intensities of C_3O and C_5O reported by Cernicharo et al. (2021b), see Table 3. In practice, the H_2 volume density and the C_3O (C_5O) column density that best fit the observations are determined by minimizing the χ^2-parameter[5] computed as follows:

$$\chi^2 = \sum_{i=1}^{n} \left(\frac{W_i^{obs} - W_i^{cal}}{\sigma_i} \right)^2 . \quad (5)$$

We show in Fig. 5 the dependence on H_2 volume density and C_3O (C_5O) column density of the χ^2-parameter for a kinetic temperature of 10 ± 2 K. For both models, few C_3O (C_5O) column density values allow to reproduce the observations with confidences better than 20% and 68%. In addition, both models predict very similar column densities. For example, within a confidence of 20% the models suggest $N = [4.0 - 9.5] \times 10^{11}$ cm^{-2} for C_3O and $N = [0.8 - 1.0] \times 10^{10}$ cm^{-2} for C_5O. It is worth noting that these column densities, especially in the case of Model (2) for C_5O, do not coincide with the typical gas density for molecular clouds such as TMC-1. Indeed, Model (2) is able to reproduce the C_5O integrated intensities for $n = [1-4]\times10^4$ cm^{-3} only within confidences greater

[5] W_i^{cal} and W_i^{obs} are the integrated intensities retrieved form our calculations and the observations, respectively. σ_i stands for the uncertainties on W_i^{obs} and the subscript n refers to the number of observed emission lines.

Table 4. Column densities (cm^{-2}) and C_3O/C_5O abundance ratios computed using both models in comparison with the data reported in the literature.

Molecule	Model (1W/E)	Model (2)	Observation*
C_3O	$[3.8-5.9]\times10^{11}$	$[4.8-6.8]\times10^{11}$	$[1.2\pm0.2]\times10^{12}$
C_5O	$[8.4-9.4]\times10^{9}$	$[1.1-1.3]\times10^{10}$	$[1.5\pm0.2]\times10^{10}$
C_3O/C_5O	40 – 70	37 – 62	80 ± 2

* stands for Cernicharo et al. (2021b)

than 90%. Such contour plots correspond to $1.6\times\sigma$ (Lampton et al. 1976) which is reasonably good for astrophysical modelling.

Concerning the H_2 volume density, the models lead to very different values. For instance, using Model (1W) and Model (2) for C_3O, we derived $n = [0.2-10]\times10^4$ cm^{-3} and $n = [1.5-10]\times10^4$ cm^{-3}, respectively adopting a confidence level of 90%. In the case of C_5O, Model (1E) suggests $n = [0.32-10]\times10^4$ cm^{-3} whereas Model (2) predicts $n = [3.12-10]\times10^4$ cm^{-3}. Calling back the fact that a volume density of $\sim 4\times10^4$ cm^{-3} is often used in the literature for TMC-1, we can affirm that Model (2) better constrains the physical conditions.

Assuming a volume density of 4×10^4 cm^{-3}, and a gas kinetic temperature of 10 ± 2 K and a confidence level of 90%, Model (2) leads to column densities of $[1.5-8.2]\times10^{11}$ cm^{-2} and $[1.1-1.3]\times10^{10}$ cm^{-2} for C_3O and C_5O, respectively. The large interval obtained in the case of C_3O can be reduced to $[4.8-6.8]\times10^{11}$ cm^{-2} adopting a confidence level of 20%. Therefore, we compare in Table 4 the results obtained for C_3O and C_5O adopting for each molecule the best fit (i.e. confidence levels of 20% and 90%, respectively). Model (1W/E) underestimates the column densities derived using Model (2) by 20 – 30% whereas the C_3O/C_5O abundance ratios differ only by $\sim$ 10%. Therefore, the greater the rate coefficients are, the smaller the column densities are.

With respect to the observations, shown in the fourth column of Table 4, Model (2) underestimates the column densities by up to 25% and accordingly the abundance ratio by up to 50%. These differences may come from the fact the observational spectra were analysed by mean of rotational diagram (Cernicharo et al. 2021b) whereas non-LTE calculations (Model (2)) are used in this work. An alternative source of bias is the omission of the filling factor in this work but its inclusion could also increase the disagreement. However, exact determination of column densities is beyond the scope of this work, but it can be done using the new rate coefficients and a more sophisticated model.

4 CONCLUSION

Integral inelastic cross sections of C_3O (C_5O) induced by collision with He were determined using the exact close-coupling quantum mechanical approach for total energies up to 750 (650) cm^{-1}. The thermal average of the cross sections by mean of the Maxwell–Boltzmann velocity distribution lead to downward rate coefficients for temperatures up to 100 K. Typically, we computed collisional rate coefficients for the 31 low-lying rotational levels of C_3O and C_5O. The comparison of the collisional data of these molecules with those of HC_3N (Green & Chapman 1978; Wernli et al. 2007) and HC_5N (obtained using equation 4) revealed that the excitation of HC_nN is much stronger than that of C_nO.

We also performed non-LTE radiative transfer calculations by mean of the `RADEX` computer code using the different sets of collisional rate coefficients mentioned above. We showed that the use of the scattering data of HC_nN instead of the actual ones can lead to LTE for gas densities as low as $\sim 10^4$ cm^{-3} and $\sim 10^3$ cm^{-3} for C_3O and C_5O, respectively. This behaviour is a direct consequence of the dominance of the HC_nN collisional rate coefficients over those of C_nO.

For the analysis of the C_3O and C_5O emission lines detected towards TMC-1 (Cernicharo et al. 2021b), the use of HC_nN as template for C_nO underestimates the column densities by up to 30%. Concerning the interpretation of the observational spectra, our non-LTE modelling which is based on the actual C_nO collisional rate coefficients reduced the column densities reported by Cernicharo et al. (2021b) down to 25% and accordingly the C_3O/C_5O abundance ratio down to 50%. Nevertheless, further non-LTE modellings that take into account the source size and the telescope efficiency are needed to draw a more consistent conclusion.

CONFLICTS OF INTEREST

There are no conflicts to declare.

DATA AVAILABILITY

The data underlying this article are available in the article. We did not consider the isotopic substitution in this work but the collisional rate coefficients of any isotopologue of C_3O and C_5O can be obtained upon request to the authors.

REFERENCES

Alexander M. H., 1977, J. Chem. Phys., 67, 2703
Bop C. T., Lique F., Faure A., Quintas-Sánchez E., Dawes R., 2021, MNRAS, 501, 1911
Brown R. D., et al., 1985, ApJ, 297, 302
Brünken S., Kluge L., Stoffels A., Asvany O., Schlemmer S., 2014, ApJ, 783, L4
Cecchi-Pestellini C., Bodo E., Balakrishnan N., Dalgarno A., 2002, ApJ, 571, 1015
Cernicharo J., et al., 2021a, A&A, 648, L3
Cernicharo J., Agúndez M., Cabezas C., Tercero B., Marcelino N., Fuentetaja R., Pardo J. R., de Vicente P., 2021b, A&A, 656, L21
Endres C. P., Schlemmer S., Schilke P., Stutzki J., Müller H. S., 2016, J. Mol. Spect., 327, 95
Filliben J. J., Heckert A., 2002, NIST, Gaithersburg
Friberg P., Hjalmarson A., Guélin M., Irvine W., 1980, ApJ, 241, L99
Green S., Chapman S., 1978, ApJS, 37, 169
Green S., Thaddeus P., 1976, ApJ, 205, 766
Guélin M., Neininger N., Cernicharo J., 1998, arXiv preprint astro-ph/9805105
Heijmen T. G., Moszynski R., Wormer P. E., Van Der Avoird A., 1997, J. Chem. Phys., 107, 9921
Hernández Vera M., Lique F., Dumouchel F., Hily-Blant P., Faure A., 2017, MNRAS, 468, 1084
Huang X., Fortenberry R. C., Lee T. J., 2013, ApJ, 768, L25
Hutson J. M., Green S., Molscat computer code, version 14 (MAR 95), distributed by Collaborative Computational Project No. 6 of the Science and Engineering Research Council (UK)
Khadri F., Hammami K., 2019, Phys. Chem. Chem. Phys., 21, 4606
Khadri F., Chefai A., Hammami K., 2020, MNRAS, 498, 5159
Khadri F., Chefai A., Hammami K., 2022, MNRAS, 513, 4573
Lampton M., Margon B., Bowyer S., 1976, ApJ, 208, 177
Matthews H. E., Irvine W. M., Friberg P., Brown R. D., Godfrey P. D., 1984, Nature, 310, 125
Ndaw D., Bop C. T., Dieye G., Faye N. B., Lique F., 2021, MNRAS, 503, 5976
Palumbo M. E., Leto P., Siringo C., Trigilio C., 2008, ApJ, 685, 1033

Pety J., et al., 2012, A&A, 548, A68
Sahnoun E., Ben Khalifa M., Khadri F., Hammami K., 2020, Ap&SS, 365, 1
Snell R., Schloerb F., Young J., Hjalmarson A., Friberg P., 1981, ApJ, 244, 45
Tenenbaum E. D., Apponi A. J., Ziurys L. M., Agúndez M., Cernicharo J., Pardo J. R., Guélin M., 2006, ApJ, 649, L17
Van der Tak F., Black J. H., Schöier F., Jansen D., van Dishoeck E. F., 2007, A&A, 468, 627
Vastel C., Ceccarelli C., Lefloch B., Bachiller R., 2014, ApJ, 795, L2
Wernli M., Wiesenfeld L., Faure A., Valiron P., 2007, A&A, 464, 1147

APPENDIX A: FULL SET OF THE STATE-TO-STATE INELASTIC COLLISIONAL RATE COEFFICIENTS

In this section, we present the variation of state-to-state rate coefficients of C_3O and C_5O induced by collision with He for temperatures of up to 100 K. For both collisional systems, the rate coefficients increase with the temperature increase. Apart from the $1 \rightarrow 0$ de-excitation, minor differences (less than a factor of 2) exist between the other $\Delta j = 1$ transitions especially at high temperature where they are all piled up. Despite these similarities, one can see that the C_5O-rate coefficients increase as a function of j whereas the transitions are mixed in the case of C_3O.

This paper has been typeset from a TEX/LATEX file prepared by the author.

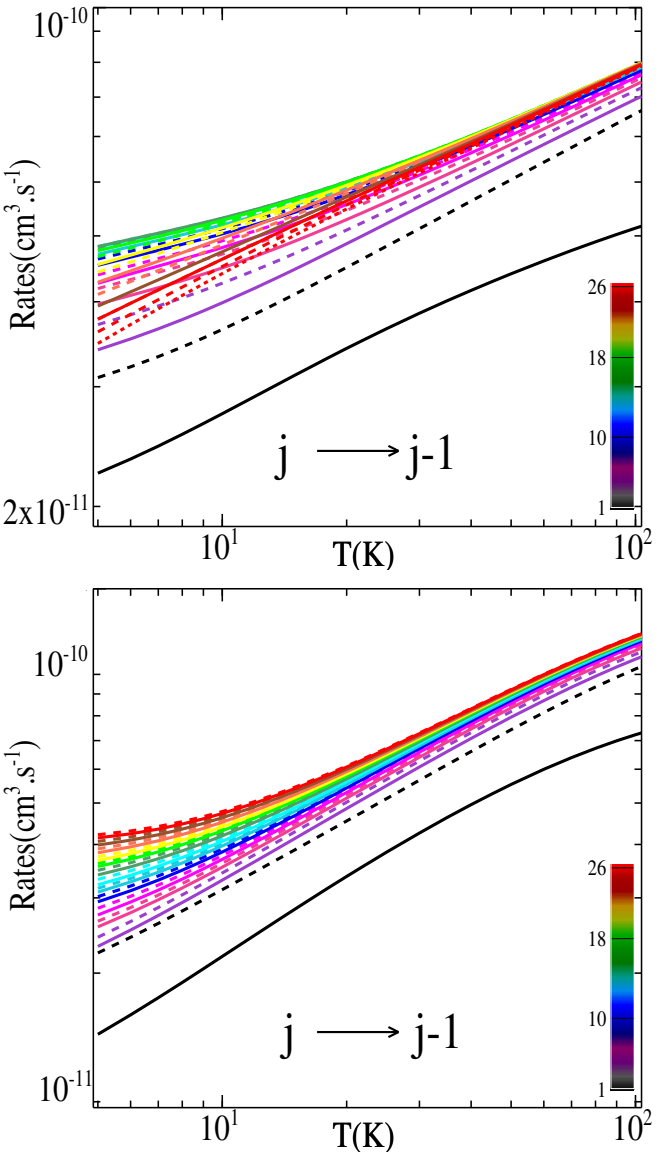

Figure A.1. Temperature dependence of rate coefficients of C_3O (up panel) and C_5O (low panel) in collision with He for $j \rightarrow j-1$ transitions, with $1 \leq j \leq 30$.